Research Square

Preprints are preliminary reports that have not undergone peer review.
They should not be considered conclusive, used to inform clinical practice,
or referenced by the media as validated information.

BET Inhibition Enhances Chemotherapy-Induced Antitumor Immunity by Limiting Macrophage Recruitment in Triple-Negative Breast Cancer

Songyin Huang

huangsy@mail.sysu.edu.cn

Sun Yat-Sen Memorial Hospital, Sun Yat-Sen University https://orcid.org/0000-0002-9575-044X

Yue Chen
Jiawei Wang
Jueqiong Xu
Yaofeng Zhou
Tengyao Wang
Jiajun Huang
Fuxiang Wang
Huosheng Zhou
Qiang Liu
Yan Bao

Article

Keywords:

Posted Date: November 12th, 2026

DOI: https://doi.org/10.21203/rs.3.rs-11432116/v1

License: This work is licensed under a Creative Commons Attribution 4.0 International License.
Read Full License

Additional Declarations: There is **NO** Competing Interest.

Abstract

Background

Chemotherapy can promote antitumor immunity in part by inducing immunogenic forms of tumor cell death, providing a rationale for combining cytotoxic agents with immunomodulatory therapies. However, chemotherapy-treated tumors may also develop myeloid-dominated microenvironments that restrict effective T cell responses. Here, we investigated whether bromodomain and extraterminal domain inhibition (BETi) could improve the immune response elicited by liposomal doxorubicin (Doxil) in triple-negative breast cancer (TNBC).

Methods

We evaluated JQ1 combined with Doxil in orthotopic 4T1 and EMT6 TNBC models, with other BET inhibitors and cisplatin used to examine broader applicability. Transcriptomic profiling, flow cytometry, immunofluorescence, and molecular assays characterized immune responses. T cell depletion, nude mice, and tumor rechallenge assessed immune dependence and memory. Macrophage recruitment was investigated using tumor profiling and in vitro migration assays.

Results

JQ1 enhanced Doxil-mediated tumor control in both models, prolonged survival in 4T1 mice, and induced complete, recurrence-free regression in EMT6 mice following repeated treatment. Additional BET inhibitors also enhanced chemotherapy efficacy. Antitumor benefit was lost in nude mice and attenuated by CD8 + T cell depletion. Combination treatment increased intratumoral T cell infiltration and activation, effector memory responses, granzyme B expression, and tumor apoptosis, while conferring resistance to rechallenge. JQ1 can reduce chemotherapy-associated macrophage accumulation, decreased CD206 and increased CD86 expression, and inhibited macrophage migration toward CCL2 and chemotherapy-treated tumor cells.

Conclusions

These findings suggest that BETi can improve chemotherapy-induced antitumor immunity by limiting macrophage recruitment and thereby creating a tumor microenvironment more permissive for $CD8^+$ T cell-mediated tumor control.

INTRODUCTION

Chemotherapy combined with immune checkpoint blockade (ICB) has become an important treatment strategy for triple-negative breast cancer (TNBC) [1–3]. In high-risk early-stage disease, pembrolizumab

plus neoadjuvant chemotherapy improves pathological complete response and event-free survival [4], and in PD-L1–positive advanced TNBC, chemotherapy–immunotherapy regimens have improved outcomes in selected patients [5]. These clinical advances further verify synergistically improved antitumor efficacy from combining baseline cytotoxic chemotherapy with immunomodulation. Mechanistically, Cytotoxic chemotherapy can induce immunogenic cell death (ICD) of tumor cell, promote danger signal release, enhance antigen presentation, and facilitate T cell priming [6–8]. However, clinical benefit remains heterogeneous and many tumors fail to develop durable immune-mediated control [9], suggesting that chemotherapy-induced antitumor immunity is frequently constrained by the tumor microenvironment.

Recent studies indicate that Chemotherapy-induced tissue damage can also activate repair programs dominated by myeloid cells [10, 11]. Chemotherapy-treated tumors frequently accumulate monocytes and tumor-associated macrophages (TAMs) [12, 13], driven in part by chemokine pathways such as CCL2–CCR2 and by factors released from dying or stressed tumor cells. Recruited macrophages can clear apoptotic cells, produce immunosuppressive cytokines, express inhibitory ligands, remodel extracellular matrix, and restrict cytotoxic T cell infiltration and function [14–18]. These findings suggest that chemotherapy may generate an immune-stimulatory window that is attenuated by a compensatory macrophage response [19]. However, strategies to preserve the T cell–promoting effects of chemotherapy while limiting treatment-associated macrophage accumulation remain incompletely defined.

Bromodomain and extra-terminal domain (BET) proteins, especially BRD4, regulate enhancer-dependent transcriptional programs involved in oncogenic signaling, inflammation, and immune cell function [20–22]. BET inhibitor (BETi) such as JQ1 have been widely studied as tumor-intrinsic transcriptional inhibitors, including in TNBC, but their immunomodulatory effects are increasingly recognized [23]. BETi can regulate inflammatory cytokine expression, antigen presentation, immune checkpoint pathways, and myeloid cell activation [24, 25]. Given the aforementioned regulatory potential of BET, we reasoned that BETi might modulate the macrophage response elicited by chemotherapy and thereby improve chemotherapy-induced antitumor immunity.

In this study, we examined the interaction between BETi and liposomal doxorubicin (Doxil) in TNBC models [26–28]. JQ1 enhanced the antitumor activity of Doxil in 4T1 and EMT6 tumor models, and the effect relied mainly on $CD8^+$ T cells. Combination therapy increased intratumoral T cell infiltration and activation, promoted effector memory responses, enhanced perforin and granzyme-associated cytotoxic programs, and was associated with sustained tumor cell apoptosis and tumor rechallenge resistance. JQ1 also reduced TAM accumulation after Doxil treatment and suppressed macrophage chemotaxis in vitro. These findings suggest that BETi can improve Doxil-induced antitumor immunity by limiting macrophage recruitment and favoring $CD8^+$ T cell-mediated tumor control.

RESULTS

2.1 BETi potentiates chemotherapy and supports durable tumor control in TNBC models

To explore whether BETi could be used to improve chemotherapy response in TNBC, we first examined BRD4 expression in breast cancer using TCGA datasets [29]. BRD4 was significantly upregulated in breast cancer tissues compared with normal breast tissues, with higher expression observed in TNBC samples (Supplemental Fig. 1, A and B). Given the established role of BET proteins in oncogenic transcription and immune-inflammatory gene regulation [30, 31], these data provided a rationale to evaluate BET inhibition as a potential chemotherapy-modulating strategy in TNBC.

We initially tested this strategy using Doxil, an anthracycline formulation with known immune-modulating potential, in an orthotopic 4T1 TNBC model. Tumor-bearing mice were randomized to receive PBS, Doxil, JQ1, or Doxil plus JQ1 according to the treatment schedule shown in Fig. 1A. Doxil alone delayed tumor growth, whereas JQ1 monotherapy produced a more limited antitumor effect. In contrast, the combination of Doxil and JQ1 resulted in substantially stronger tumor suppression than either single agent, as shown by reduced tumor growth, smaller excised tumors, and decreased tumor weight (Fig. 1, B-D). Combination therapy also prolonged survival of 4T1 tumor-bearing mice (Fig. 1E). Importantly, this improved antitumor activity was not accompanied by obvious systemic toxicity under the tested conditions: body weight remained stable across treatment groups, serum levels of alanine aminotransferase (ALT), aspartate aminotransferase (AST), and blood urea nitrogen (BUN) showed no evident hepatic or renal injury, and histological examination of major organs revealed no apparent tissue damage (Supplemental Fig. 2, A-C). These results established that BETi can improve the therapeutic index of Doxil in an immunocompetent TNBC model.

To determine whether the benefit of BETi was specific to Doxil or could extend to other chemotherapeutic agents, we tested JQ1 in combination with cisplatin (CDDP) [32, 33]. Platinum-based chemotherapy is clinically relevant in TNBC, particularly in neoadjuvant and selected advanced-disease settings, and has been associated with improved pathological complete response rates when incorporated into chemotherapy regimens [34, 35]. Orthotopic 4T1 tumor-bearing mice were treated with CDDP alone or CDDP plus JQ1 according to the schedule shown in Fig. 1F. JQ1 significantly enhanced the tumor growth inhibition induced by CDDP (Fig. 1G), indicating that BETi can cooperate with chemotherapy beyond the Doxil setting.

We further examined whether this effect was unique to JQ1 or could be observed with additional BET inhibitors. Two BET inhibitors with different pharmacological profiles, OTX-015 and RVX-208, were evaluated in combination with Doxil in the orthotopic 4T1 model [36, 37]. Both inhibitors improved Doxil-mediated tumor suppression, with OTX-015 showing stronger antitumor activity than RVX-208 under the tested conditions (Fig. 1, H and I). These findings suggest that chemotherapy enhancement is not restricted to a single BETi, although the magnitude of benefit may differ among BET-targeting agents.

We next asked whether this therapeutic enhancement could be reproduced in orthotopic EMT6 tumors. Doxil plus JQ1 again produced the most pronounced tumor growth suppression during long-term observation (Fig. 1J). Because durable disease control is a major limitation of chemotherapy-based

treatment, we further evaluated whether repeated chemotherapy administration would improve response durability [38]. EMT6 tumor-bearing mice received either two or four administrations of Doxil, with or without JQ1. Increasing the number of Doxil doses improved tumor resolution in both the Doxil monotherapy and combination groups. However, the most durable responses were observed in the Doxil plus JQ1 group. After four Doxil administrations, all mice receiving the combination achieved complete tumor regression, and no recurrence was detected during the 60-day post-treatment monitoring period (Fig. 1K). The recurrence-free complete responses in this immunocompetent model suggested that BETi may do more than transiently increase chemotherapy cytotoxicity; rather, it may help convert chemotherapy response into more durable tumor control.

Together, these results show that BETi universally boosts chemotherapy efficacy in TNBC models, and the sustained tumor regression with no recurrence in repeatedly dosed EMT6 tumors implies this combination acts via host-dependent mechanisms beyond direct cytotoxicity, prompting further exploration of tumor microenvironment immune remodeling.

2.2 Doxil plus JQ1 induces immune-associated remodeling transcriptional and requires T cell immunity for better therapeutic efficacy

To investigate mechanisms underlying the enhanced therapeutic activity of Doxil plus JQ1, we performed RNA-seq analysis of 4T1 tumor tissues collected after treatment (Fig. 2A). Compared with Doxil monotherapy, tumors treated with Doxil plus JQ1 showed enrichment of immune- and inflammation-related transcriptional programs by Hallmark gene set-based GSEA, including pathways associated with inflammatory responses and complement activation (Fig. 2B). KEGG pathway analysis and KEGG-based GSEA further identified enrichment of immune-related pathways in the combination group relative to Doxil alone (Fig. 2, C and D). Consistently, GSVA across all treatment groups showed that Doxil plus JQ1 was associated with higher enrichment scores for multiple immune and inflammatory hallmark pathways than PBS, JQ1, or Doxil treatment alone (Fig. 2E). These transcriptomic changes suggested that JQ1 altered the tumor response to Doxil toward a more immune-inflamed state.

We next estimated immune cell abundance from the transcriptomic profiles using mMCPcounter [39]. Tumors treated with Doxil plus JQ1 showed increased inferred abundance of T cells, $CD8^+$ T cells, and NK cells compared with the other treatment groups (Fig. 2F). In parallel, cytokine antibody array analysis of 4T1 tumor tissues revealed increased levels of several cytokines and chemoattractants in the combination group, including RANTES, IL-4, IL-1α/β, MIP-1α/β, and IL-12p40 (Fig. 2G). Although these factors have diverse immunological functions, their coordinated increase was consistent with a broader remodeling of the intratumoral inflammatory and immune-recruitment milieu after Doxil plus JQ1 treatment. Together, these transcriptional and cytokine-level analyses indicated that the combination therapy was associated with enhanced immune-inflammatory remodeling within the tumor microenvironment. To determine whether the immune system was functionally required for the improved antitumor efficacy, we evaluated the combination therapy in BALB/c nude mice bearing 4T1 tumors. In contrast to the results observed in immunocompetent mice, JQ1 failed to improve the antitumor activity

of Doxil in nude mice (Fig. 2H and Supplemental Fig. 3), indicating that host immunity is necessary for the full therapeutic benefit of the combination. We further assessed the contribution of T cell subsets using antibody-mediated depletion. Depletion of either $CD4^+$ or $CD8^+$ T cells attenuated the antitumor effect of Doxil plus JQ1, with $CD8^+$ T cell depletion producing a more pronounced reduction in efficacy. Concurrent depletion of both $CD4^+$ and $CD8^+$ T cells nearly abolished the enhanced therapeutic effect of the combination (Fig. 2I). These results demonstrate that the improved efficacy of Doxil plus JQ1 depends substantially on adaptive antitumor immunity, with $CD8^+$ T cells playing a dominant role.

Collectively, these data indicate that Doxil plus JQ1 reshapes the tumor microenvironment toward an immune-inflamed state and that the enhanced therapeutic efficacy of the combination requires adaptive immunity, particularly $CD8^+$ T cells. We therefore next examined whether the combination directly altered intratumoral T cell infiltration, activation, and memory-associated responses.

2.3 Doxil plus JQ1 enhances T cell infiltration and promotes memory-associated antitumor responses

Given the requirement for T cells in the therapeutic efficacy of Doxil plus JQ1, we next examined whether the combination altered the abundance and phenotype of T cells within the tumor microenvironment over the course of treatment. Tumor tissues were collected at defined time points for flow cytometric analysis, with the gating strategy shown in Supplemental Fig. 4A and the experimental schedule shown in Fig. 3A. Compared with Doxil monotherapy, Doxil plus JQ1 increased the number of intratumoral $CD3^+$ T cells, with the most prominent increase observed at day 4 after treatment initiation (Fig. 3, B and C; Supplemental Fig. 4B). Immunofluorescence analysis further supported enhanced T cell infiltration in tumors from the combination group (Supplemental Fig. 5).

We then assessed major T cell subsets within the tumor. Both $CD8^+$ and $CD4^+$ T cells increased earlier and remained at higher levels after treatment in tumors from mice receiving Doxil plus JQ1 compared with Doxil alone (Fig. 3, D and E; Supplemental Fig. 4, C and D). Immunofluorescence staining of tumor sections collected on day 13 confirmed increased $CD3^+$ and $CD8^+$ T cell infiltration in the combination group (Fig. 3, F and G). These results indicate that JQ1 enhances the ability of Doxil-treated tumors to accumulate T cells, including cytotoxic $CD8^+$ T cells, rather than merely altering transcriptional immune signatures.

We next evaluated whether increased T cell infiltration was accompanied by phenotypic evidence of activation. CD69 expression on intratumoral $CD8^+$ T cells was significantly increased in the Doxil plus JQ1 group compared with monotherapy groups (Fig. 3H and Supplemental Fig. 4E), indicating a more activated $CD8^+$ T cell state within the tumor. Importantly, this increase in T cell infiltration and activation was not accompanied by a detectable expansion of regulatory T cells under the tested conditions (Supplemental Fig. 4F). Thus, combination treatment was associated with a shift toward increased effector T cell presence and activation within the tumor microenvironment.

Because durable tumor control after chemotherapy may require immune responses that persist beyond the initial treatment window, we further analyzed memory-associated T cell populations [40]. On day 13, splenic $CD4^+$ and $CD8^+$ effector memory T cells were increased in mice treated with Doxil plus JQ1 compared with control or monotherapy groups (Fig. 3, I and J). To functionally assess whether the combination treatment generated protection against tumor re-exposure, mice from each treatment group underwent surgical resection of primary tumors on day 9, followed by 4T1 tumor cell rechallenge four weeks later. Mice previously treated with Doxil plus JQ1 showed the strongest resistance to rechallenge, with tumor formation observed in only one mouse within the monitoring period shown (Fig. 3K). These findings suggest that the combination therapy not only enhances local T cell infiltration and activation during treatment but also promotes memory-associated antitumor responses capable of limiting subsequent tumor outgrowth.

Together, these data extend the immune-dependence findings from Fig. 2 by showing that Doxil plus JQ1 increases intratumoral T cell accumulation, enhances $CD8^+$ T cell activation, and is associated with systemic effector memory T cell expansion and improved resistance to tumor rechallenge. These observations support a model in which BETi helps convert the immune response elicited by Doxil into a more sustained T cell-mediated antitumor response.

2.4 Doxil plus JQ1 enhances cytotoxic effector programs and sustains tumor cell apoptosis

Having observed increased infiltration and activation of intratumoral T cells after Doxil plus JQ1 treatment, we next examined whether the combination was associated with enhanced cytotoxic effector activity. Further analysis of the RNA-seq dataset revealed that multiple granzyme family genes, including Gzmb, Gzmc, Gzmd, Gzme, Gzmf, Gzmg, Gzmk, and Gzmn, were upregulated in tumors treated with Doxil plus JQ1 compared with Doxil alone. The cytotoxic effector molecule Prf1, which encodes perforin, was also increased in the combination group (Fig. 4, A and B). qRT-PCR analysis of tumor tissues collected at an earlier treatment stage further validated the increased expression of granzyme family genes and Prf1 after Doxil plus JQ1 treatment (Fig. 4C). In parallel, immunofluorescence and immunohistochemical staining showed increased intratumoral granzyme B signal in the combination group (Fig. 4, D-F). These findings indicate that Doxil plus JQ1 enhances a granzyme- and perforin-associated cytotoxic effector program within the tumor microenvironment.

To place these observations in a clinically relevant context, we analyzed the association between granzyme family gene expression and patient outcome in TNBC using TCGA datasets. Higher expression of several granzyme family genes was associated with improved prognosis in TNBC patients (Fig. 4G). Although this analysis does not establish causality, it supports the clinical relevance of cytotoxic immune effector signatures in TNBC and is consistent with the enhanced granzyme-associated program observed in tumors treated with Doxil plus JQ1.

Because granzymes and perforin are key effector molecules used by cytotoxic lymphocytes to induce target-cell death, we next assessed whether the enhanced cytotoxic program was accompanied by increased tumor cell death during treatment. Tumor tissues were collected at defined time points

according to the schedule shown in Fig. 5A. H&E staining revealed more pronounced histopathological damage in tumors from the combination group, including nuclear pyknosis and fragmentation, expanded interstitial spaces, and increased necrotic or vacuolated regions (Fig. 5B). Transcriptomic pathway analysis further showed that, compared with Doxil monotherapy, Doxil plus JQ1 was associated with downregulation of proliferation- and cell cycle-related programs, including MYC targets, E2F targets, G2M checkpoint, mitotic pathways, and DNA repair pathways (Fig. 5C). These data suggest that the combination treatment imposes stronger suppression of tumor proliferative programs than Doxil alone.

We then evaluated regulated cell death-associated signatures. ssGSEA analysis showed increased enrichment scores for several cell death-related pathways in the Doxil plus JQ1 group, including apoptosis, ferroptosis, pyroptosis, and necroptosis [41] (Fig. 5D). Among these, apoptosis was further examined experimentally. Western blot analysis demonstrated increased cleaved caspase-3 levels in tumor tissues from the combination group on day 13 (Fig. 5, E and F). TUNEL staining further showed that apoptotic cells remained elevated in tumors treated with Doxil plus JQ1 at later time points, including day 20 (Fig. 5G). These results indicate that the combination treatment is associated with increased and sustained apoptotic tumor cell death.

Together, these data show that Doxil plus JQ1 enhances intratumoral granzyme- and perforin-associated cytotoxic effector programs and is accompanied by sustained tumor apoptosis. In the context of the increased $CD8^+$ T cell infiltration and activation described above, these findings support a model in which BETi strengthens chemotherapy-associated cytotoxic antitumor immunity, although functional blockade studies would be required to determine whether the perforin-granzyme axis is directly required for the observed apoptosis.

2.5 BETi suppresses macrophage chemotaxis and reduces post-treatment TAM accumulation

Given that chemotherapy-induced tumor cell death can be accompanied by remodeling of myeloid cell populations, we next examined whether Doxil plus JQ1 altered tumor-associated macrophages (TAMs) in parallel with the T cell changes described above. Using the same treatment time points applied for T cell analysis, tumor tissues were collected for flow cytometric quantification of macrophage populations and phenotypic markers (Fig. 6A and Supplemental Fig. 6A). Compared with Doxil monotherapy, Doxil plus JQ1 reduced the number of intratumoral macrophages (Fig. 6B and Supplemental Fig. 6B). In addition, macrophages from the combination group showed decreased expression of CD206 and increased expression of CD86 (Fig. 6, C and D; Supplemental Fig. 6C). Although these markers do not fully define macrophage function, the observed changes suggest that JQ1 treatment reduces macrophage accumulation and alters macrophage-associated phenotypic features within Doxil-treated tumors.

Because TAMs can be replenished by circulating monocytes recruited into tumor tissues, we next analyzed peripheral blood myeloid populations during treatment [12, 42]. In contrast to the reduced macrophage abundance observed within tumors, the proportions of circulating monocytes/macrophage-related populations were increased in mice receiving Doxil plus JQ1 (Fig. 6, E and F; Supplemental Fig. 6,

D-F). This inverse relationship between peripheral and intratumoral myeloid populations suggested that BETi may interfere with the recruitment of monocyte/macrophage-lineage cells into tumors after chemotherapy, rather than simply depleting these cells systemically.

To directly test whether BETi affected macrophage migratory capacity, we performed in vitro migration assays using bone marrow-derived macrophages (BMDMs). JQ1 was first evaluated at concentrations that did not markedly compromise BMDM viability under the tested conditions (Supplemental Fig. 7). Transwell assays showed that JQ1 significantly reduced BMDM migration (Fig. 6G). In the presence of the chemoattractant CCL2, multiple BET inhibitors, including JQ1, OTX-015, and RVX-208, consistently suppressed macrophage chemotaxis (Fig. 6, H-J), suggesting that inhibition of macrophage migration is not unique to JQ1. Scratch wound assays using Raw264.7 murine macrophages further showed that JQ1 impaired macrophage motility in an independent migration model (Fig. 6, K and L).

We next assessed whether BETi could counteract tumor cell-driven macrophage recruitment in the context of chemotherapy. In a Transwell coculture system, Doxil-treated 4T1 tumor cells modestly increased macrophage migration toward tumor cells. Addition of JQ1 reduced this Doxil-associated macrophage recruitment (Fig. 6, M and N). These data indicate that BETi can limit macrophage chemotaxis driven by chemotherapy-treated tumor cells, providing a potential explanation for the reduced TAM accumulation observed in vivo after Doxil plus JQ1 treatment.

Together, these findings show that BETi reduces post-treatment TAM accumulation and suppresses macrophage migratory responses in vitro. In the context of the enhanced T cell infiltration and cytotoxic effector programs described above, these results support a model in which JQ1 helps remodel the post-chemotherapy tumor microenvironment by limiting macrophage recruitment and decreasing macrophage-associated immunosuppressive features. However, additional functional rescue or macrophage-specific perturbation studies would be required to determine the extent to which reduced TAM recruitment directly accounts for the enhanced T cell-mediated antitumor efficacy of Doxil plus JQ1.

DISCUSSION

This study suggests that BETi can improve the immune miacroenvironment in which chemotherapy acts in TNBC. Rather than functioning only as a tumor-intrinsic chemosensitizer, JQ1 enhanced Doxil efficacy in immunocompetent models in a manner that required T cells, particularly $CD8^+$ T cells. The combination was associated with increased T cell infiltration and activation, induction of granzyme/perforin-associated cytotoxic programs, sustained tumor apoptosis, and resistance to tumor rechallenge. These findings support a model in which BETi helps convert chemotherapy-induced tumor injury into a more effective T cell-supported antitumor response.

A central feature of this combination strategy lies in its ability to restrict macrophage recruitment after chemotherapy. Doxil plus JQ1 reduced intratumoral macrophage accumulation while increasing circulating monocyte/macrophage-lineage populations, and BETi directly impaired macrophage

migration in vitro. These observations suggest that BETi limits the entry of macrophage-lineage cells into the post-chemotherapy tumor microenvironment, rather than simply eliminating them systemically. This is consistent with previous reports linking BET proteins to inflammatory transcriptional programs controlling chemokine receptor expression, macrophage trafficking, and cytoskeletal regulation. The precise molecular mechanism underlying this migratory defect remains to be elucidated.

The reduction in macrophage recruitment may help explain why chemotherapy-induced tumor damage becomes more immunologically productive in the presence of BETi. Macrophages recruited to dying tumors can participate in apoptotic cell clearance and immunoregulatory remodeling, processes that may dampen cytotoxic T cell responses. In our study, residual macrophages after combination treatment showed reduced CD206 and increased CD86 expression, suggesting a shift in macrophage-associated phenotypic features. Although these data do not prove functional repolarization or impaired efferocytosis [43–46], they indicate that BETi reshapes the myeloid compartment in a direction compatible with enhanced T cell activity.

The prominence of granzyme family genes and Prf1 further links this remodeled microenvironment to cytotoxic immunity [47, 48]. The combination increased granzyme B signal and was accompanied by cleaved caspase-3 activation and persistent TUNEL positivity, suggesting that enhanced cytotoxic effector programs coincide with sustained tumor apoptosis. However, because perforin or granzyme blockade was not performed, the perforin–granzyme axis should be viewed as an associated effector program, not as the sole proven cause of tumor cell death.

Together, these findings position BETi as an immune-oriented adjunct to chemotherapy. By limiting post-treatment macrophage recruitment while supporting T cell infiltration, cytotoxic effector activity, and memory-associated protection, BET inhibitors may broaden the therapeutic window of chemotherapy in TNBC. Future work should define the molecular basis of macrophage migration control, the optimal timing of BETi relative to chemotherapy, and whether this strategy can be extended to other tumors in which myeloid remodeling limits durable response.

MATERIALS AND METHODS

Tumor cell lines

Murine breast carcinoma cell lines (4T1, EMT6) were obtained from the American Type Culture Collection (ATCC, Manassas, VA, USA). All cell lines were cultured in DMEM medium supplemented with 10% fetal bovine serum (FBS) and 1% penicillin-streptomycin at 37°C in a humidified atmosphere containing 5% CO_2, following the provider’s instructions.

Tumor treatments

For the breast tumou r orthotopic model (using 6-week-old female BALB/c mice) and immunodeficient nude mouse model (using 6-week-old female Nude BALB/c mice), the third right mammary fat pad was orthotopically injected with 5×10^5 4T1 cells or 3×10^5 EMT6 cells suspended in 50 μL phosphate-buffered saline (PBS), respectively.

To evaluate the co-efficacy of Doxil and BET inhibitors (BETi), tumour-bearing BALB/c mice were randomly divided into 4 groups when tumour volume reached 60–80 mm^3: (1) PBS; (2) BETi (JQ1, OTX-015, RVX-208); (3) Doxil; (4) Doxil plus BETi (JQ1, OTX-015, RVX-208). Treatments were administered as follows: Doxil (5 mg/kg, Alza Corporation, USA) was intravenously injected once on the first day of treatment; JQ1 (50 mg/kg, Selleck Chemicals, USA) was intraperitoneally injected daily for 7 days; OTX-015 (50 mg/kg, MedChemExpress, USA) and RVX-208 (200 mg/kg, MedChemExpress, USA) was intraperitoneally injected daily for 5 days. Mammary tumour volume in female mice was measured every 2–3 days using a vernier caliper, calculated as: largest diameter × $(\text{shortest diameter})^2/2$.

For tumor rechallenge experiments, mice were inoculated orthotopically with 5×10^5 4T1 cells on the flank opposite to the primary tumour, 30 days after the completion of treatment.

For $CD4^+$ and/or $CD8^+$ T cell depletion experiments, mice were intraperitoneally injected with 150 μg anti-CD8a antibody (clone 53 − 6.7, BioXCell, USA) and/or anti-CD4 antibody (clone GK1.5, BioXCell, USA) starting 2 days before tumour implantation, with injections repeated every 4 days until the end of the experiment.

All mice (6-week-old female, including wild-type BALB/c and Nude BALB/c) were purchased from Bestest Biotechnology Co., Ltd. (Zhuhai, China). The experimental protocol was approved by the Animal Ethical and Welfare Committee of Sun Yat-sen Memorial Hospital.

H&E, Immunohistochemical (IHC) and immunofluorescence (IF) staining

Tumor specimens were fixed in 4% buffered formalin at room temperature for 24–48 hours, then embedded in paraffin. 4-μm sections were prepared for H&E staining, IHC, or IF staining.

Terminal deoxynucleotidyl transferase-mediated dUTP-biotin nick end labeling (TUNEL) was performed to detect apoptotic cells using the One-Step TUNEL Kit (Cat# C1090, Beyotime Institute of Biotechnology, Shanghai, China) according to the manufacturer's instructions. TUNEL-positive cells (red fluorescence) were counted in 3 random high-power fields per section using ImageJ software (NIH, USA).

Western blot analysis

Total protein was extracted from the cells or tissues using RIPA lysis buffer, and the concentration of the supernatant was determined using a BCA™ Protein Assay Kit (Thermo Scientific) according to the

manufacturer's instructions. For SDS-PAGE, 20 μg of protein per lane was loaded onto Tris-glycine gels and electrophoresed at 90 V for 2 hours. Separated proteins were then transferred to polyvinylidene fluoride (PVDF) membranes (Millipore, USA) using a transfer buffer at a constant current of 250 mA for 1.5 hours. After electro-transfer, the membranes were blocked for 1 hour at ambient temperature in 5% non-fat milk in TBS and 0.05% Tween-20 (TBST), and then incubated with primary antibodies in TBST with 5% BSA at a 1:1000 dilution at 4°C overnight. After three washes with TBST (5 minutes each), membranes were incubated with horseradish peroxidase (HRP)-conjugated secondary antibodies for 1 hour at room temperature, followed by three additional washes with TBST. Immunoreactive bands were visualized using Omni-ECL™ chemiluminescent substrate (Epizyme, China) and imaged with a gel imaging system. The molecular sizes of proteins were determined using Prestained Protein Marker (Servicebio, China). Band intensities were quantified using ImageJ software (NIH, USA).

qRT-PCR

Quantitative reverse transcription PCR (qRT-PCR) was performed using SYBR Premix Ex Taq kit (TaKaRa, Japan) according to the manufacturer's instructions. Data were collected and analyzed with a LightCycler480 instrument (Roche). Primers for quantitative PCR with reverse transcription were listed in the Supplemental Table 1.

Preparation of single-cell suspensions

Tumour masses harvested from mice were minced into 1–2 mm^3 pieces using sterile scissors. The tissue fragments were digested in RPMI 1640 medium containing 1 mg/mL collagenase D (Ascgene), 0.1 mg/mL DNase (Biofroxx), and 0.1 mg/mL hyaluronidase (Biofroxx) at 37°C with gentle shaking (150 rpm) for 1 hour. The digested mixture was filtered through a 70 μm cell strainer (Falcon) to remove undigested debris, and the filtrate was centrifuged at 300×g for 5 minutes at 4°C to collect cells. Red blood cells were lysed by resuspending the cell pellet in 1 mL erythrocyte lysis buffer and incubating on ice for 10 minutes. The single-cell suspension was washed and resuspended in PBS.

Flow cytometry

For flow cytometric staining, single-cell suspensions (~ $1×10^6$ cells per sample) were incubated using fluorochrome-conjugated antibodies for 30 minutes at 4°C in the dark. Data were acquired using a Beckman CytoFLEX LX flow cytometer with CytExpert software v2.5.077 and analysed with FlowJo software v9.9.6 (BD Biosciences). Cell populations were identified using gating strategies as shown in Supplementary Figs. 4 and 6.

Bulk RNA sequencing and data analysis

Tumors were collected from the 4T1 mice treated 13 days after initiation of treatment, washed in 1×PBS twice, stored immediately in liquid nitrogen, and performed RNA isolation and sequencing by the Beijing

Genomics Institute (BGI), Shenzhen. Raw sequence reads were submitted to the National Center for Biotechnology Information (NCBI) Sequence Read Archive.

Chemotaxis assay

Bone marrow-derived macrophages (BMDMs) were cultured for 7 days in DMEM supplemented with 20 ng/mL murine M-CSF (R&D Systems, Abingdon, UK) at 37°C with 5% CO_2. For the chemotaxis assay, 24-well Falcon Transwell inserts (BD Pharmingen) were used. Briefly, the lower chamber of each Transwell was filled with 600 µL DMEM containing chemotactic factors: 20 ng/mL CCL2 or 10% FBS. BMDMs were harvested, resuspended in serum-free DMEM (with different concentration of BETi or an equal volume of DMSO as vehicle control) at a density of 1×10^6 cells/mL, and 100 µL of the cell suspension (1×10^5 cells) was added to the upper chamber. Following incubation for 24 hours, cells on the bottom surface (migrated BMDMs) of the membrane were fixed in 4% paraformaldehyde for 15 minutes. Crystal violet stain was added in PBS to the transwells. The membranes were imaged and number of macrophages was counted in five random fields.

Wound healing assay

Macrophage migration ability was further examined by the Wound healing test. RAW264.7 were plated at an appropriate density on a 60 mm dish. On the 2nd day after plating, a 200 µL sterile micropipette tip was used to scratch the cell layer. Images of the scratch were captured at 0 h (immediately after scratching) and 12 h. The number of macrophages was counted in five random fields within the scratch area, and the average value was calculated. Each group was performed in triplicate, and the experiment was repeated independently three times.

Statistical analysis

All mouse statistical measurements are displayed as mean ± SEM., otherwise as mean ± SD. P values were calculated by an unpaired two-tailed Student's t-test for two-group comparisons, by one-way ANOVA for multi-group comparisons using Prism 8.x software (GraphPad). The number of replicates performed is indicated in each figure legend, where applicable. Probability values of $P < 0.05$ were considered significant.

Declarations

ACKNOWLEDGMENTS

Ethics approval and consent to participate

All animal experiments were approved by the Animal Ethical and Welfare Committee of Sun Yat-sen Memorial Hospital (approval number: AP20230223) and were conducted in accordance with the institutional guidelines for the care and use of laboratory animals. Consent to participate was not applicable because no human participants were involved in this study.

Competing interests

The authors declare that they have no conflicts of interest related to this study.

Funding

This work was supported by the National Natural Science Foundation of China (82371856); the Guangdong Basic and Applied Basic Research Foundation (2026A1515010415); the Guangdong Provincial Key Laboratory of Cancer Pathogenesis and Precision Diagnosis and Treatment (2024B1212030002); and the Science and Technology Projects in Guangzhou (2025A03J4194).

Author contributions

Y.C., J.W. and J.X. conceived the conceptual framework and developed the methodology of this work, conducted the major experimental investigations, finished data visualization, and composed the original draft of the manuscript. J.H., T.W., F.W. and H.Z. assisted with experimental data collection and investigation, and Y.Z. took part in drafting the original manuscript. Y.B., S.H., Q.L. and Y.Y. provided full supervision throughout the whole research, participated in the formulation of research concepts and methodologies, and completed manuscript review and editing to revise the final paper. Y.C., J.W. and J.X. contributed equally to this work in both conceptual design and experimental execution.

Data availability

All data are available in the main manuscript or the Supplementary Materials. Address correspondence to: huangsy@mail.sysu.edu.cn (S. Huang), baoy5@mail.sysu.edu.cn (Y. Bao), liuq77@mail.sysu.edu.cn (Q. Liu).

References

1. Heater NK, Warrior S, Lu J. Current and future immunotherapy for breast cancer. *J Hematol Oncol*. 2024;17(1):131.
2. Schmid P, Cortes J, Dent R, Pusztai L, McArthur H, Kummel S, Bergh J, Denkert C, Park YH, Hui R, et al. Event-free Survival with Pembrolizumab in Early Triple-Negative Breast Cancer. *N Engl J Med*. 2022;386(6):556–567.
3. Schmid P, Cortes J, Dent R, McArthur H, Pusztai L, Kummel S, Denkert C, Park YH, Hui R, Harbeck N, et al. Overall Survival with Pembrolizumab in Early-Stage Triple-Negative Breast Cancer. *N Engl J Med*. 2024;391(21):1981–1991.
4. Arora A, Bhaskarane H, Tansir G, Bakhshi S, Gogia A, Kumar A, Jain R, Kalra K, Vishvam D, Mathur S, et al. A phase II, randomized, open-label study to evaluate low-dose pembrolizumab plus

chemotherapy versus chemotherapy as neoadjuvant therapy for localized triple-negative breast cancer (TNBC) (PLANeT trial-Pembrolizumab Low dose in Addition to NACT in TNBC). *Ann Oncol*. 2026;37(5):639–649.

5. Cortes J, Rugo HS, Cescon DW, Im SA, Yusof MM, Gallardo C, Lipatov O, Barrios CH, Perez-Garcia J, Iwata H, et al. Pembrolizumab plus Chemotherapy in Advanced Triple-Negative Breast Cancer. *N Engl J Med*. 2022;387(3):217–226.
6. Galluzzi L, Guilbaud E, Schmidt D, Kroemer G, Marincola FM. Targeting immunogenic cell stress and death for cancer therapy. *Nat Rev Drug Discov*. 2024;23(6):445–460.
7. Kroemer G, Galassi C, Zitvogel L, Galluzzi L. Immunogenic cell stress and death. *Nat Immunol*. 2022;23(4):487–500.
8. Zhang H, Li S, Liu S, Liao Y, Liu H, Yang M, Chen P. Therapeutic targeting of cell death-immune crosstalk in cancer to rewire the tumor immune microenvironment. *Mol Cancer*. 2025;24(1):277.
9. Koh SB, Ellisen LW. Immune activation and evolution through chemotherapy plus checkpoint blockade in triple-negative breast cancer. *Cancer Cell*. 2021;39(12):1562–1564.
10. Sung CYW, Hayase N, Yuen PST, Lee J, Fernandez K, Hu X, Cheng H, Star RA, Warchol ME, Cunningham LL. Macrophage depletion protects against cisplatin-induced ototoxicity and nephrotoxicity. *Sci Adv*. 2024;10(30):eadk9878.
11. Wang X, Pan Q, Li Y, Li N, Guo J, Gu Y, Zhang G, Lian Y, Liu H, Cao L, et al. Chemotherapy triggers immune evasion by fostering LEPR(+) Kupffer cell differentiation in liver metastases. *Cancer Cell*. 2026;44(3):658–675 e612.
12. Cassetta L, Pollard JW. A timeline of tumour-associated macrophage biology. *Nat Rev Cancer*. 2023;23(4):238–257.
13. Jiang R, Yang L, Liu X, Xu Y, Han L, Chen Y, Gao G, Wang M, Su T, Li H, et al. Genetically engineered macrophages reverse the immunosuppressive tumor microenvironment and improve immunotherapeutic efficacy in TNBC. *Mol Ther*. 2025;33(7):3339–3359.
14. Xia J, Zhang L, Peng X, Tu J, Li S, He X, Li F, Qiang J, Dong H, Deng Q, et al. IL1R2 Blockade Alleviates Immunosuppression and Potentiates Anti-PD-1 Efficacy in Triple-Negative Breast Cancer. *Cancer Res*. 2024;84(14):2282–2296.
15. Pedroza DA, Yuan X, Liu F, Chan HL, Zhang C, Bowie W, Smith AJ, Calderon SJ, Lieu N, Wu W, et al. Anti-CSF-1R therapy with combined immuno-chemotherapy coordinate an adaptive immune response to eliminate macrophage enriched triple negative breast cancers. *Nat Commun*. 2026;17(1):1193.
16. Zhu X, Liang R, Lan T, Ding D, Huang S, Shao J, Zheng Z, Chen T, Huang Y, Liu J, et al. Tumor-associated macrophage-specific CD155 contributes to M2-phenotype transition, immunosuppression, and tumor progression in colorectal cancer. *J Immunother Cancer*. 2022;10(9).
17. Peura A, Turpin R, Liu R, Heilala M, Salmela M, Aung J, Mikkonen P, Mutka M, Kovanen PE, Niinikoski L, et al. Soft matrix promotes immunosuppression in tumor-resident immune cells via COX-FGF2 signaling. *Nat Commun*. 2025;16(1):4908.

18. Chen Y, Shu X, Guo JY, Xiang Y, Liang SY, Lai JM, Zhou JY, Liu LH, Wang P. Nanodrugs mediate TAMs-related arginine metabolism interference to boost photodynamic immunotherapy. *J Control Release*. 2024;367:248–264.
19. Ruffell B, Coussens LM. Macrophages and therapeutic resistance in cancer. *Cancer Cell*. 2015;27(4):462–472.
20. Cochran AG, Conery AR, Sims RJ, 3rd. Bromodomains: a new target class for drug development. *Nat Rev Drug Discov*. 2019;18(8):609–628.
21. Delmore JE, Issa GC, Lemieux ME, Rahl PB, Shi J, Jacobs HM, Kastritis E, Gilpatrick T, Paranal RM, Qi J, et al. BET bromodomain inhibition as a therapeutic strategy to target c-Myc. *Cell*. 2011;146(6):904–917.
22. Donati B, Lorenzini E, Ciarrocchi A. BRD4 and Cancer: going beyond transcriptional regulation. *Mol Cancer*. 2018;17(1):164.
23. Shu S, Lin CY, He HH, Witwicki RM, Tabassum DP, Roberts JM, Janiszewska M, Huh SJ, Liang Y, Ryan J, et al. Response and resistance to BET bromodomain inhibitors in triple-negative breast cancer. *Nature*. 2016;529(7586):413–417.
24. Sharma D, Bushnell GG, Kalman AP, Hutchens CM, Burness ML. Bromodomain and extra-terminal proteins in solid tumors: regulators of immune microenvironment and emerging therapeutic targets. *Front Immunol*. 2025;16:1727365.
25. Zhang M, Wang G, Ma Z, Xiong G, Wang W, Huang Z, Wan Y, Xu X, Hoyle RG, Yi C, et al. BET inhibition triggers antitumor immunity by enhancing MHC class I expression in head and neck squamous cell carcinoma. *Mol Ther*. 2022;30(11):3394–3413.
26. Wang G, Wang N, Xia X, Ismail M, Shi B. Clinical translation of nanomedicines for brain diseases: Current challenges and future directions. *J Control Release*. 2026;389:114426.
27. Wang L, Luo R, Onyshchenko K, Rao X, Wang M, Menz B, Gaedicke S, Grosu AL, Firat E, Niedermann G. Adding liposomal doxorubicin enhances the abscopal effect induced by radiation/alphaPD1 therapy depending on tumor cell mitochondrial DNA and cGAS/STING. *J Immunother Cancer*. 2023;11(8).
28. Ngai J, MacMillan P, Kingston BR, Lin ZP, Ouyang B, Chan WCW. Delineating the tumour microenvironment response to a lipid nanoparticle formulation. *J Control Release*. 2023;353:988–1001.
29. Kim R, Yu J, Lim J, Oh BB, Nam SJ, Kim SW, Lee JE, Chae BJ, Kim JY, Park GE, et al. Whole-genome landscapes of 1,364 breast cancers. *Nature*. 2026;649(8099):1282–1291.
30. Wang ZQ, Zhang ZC, Wu YY, Pi YN, Lou SH, Liu TB, Lou G, Yang C. Bromodomain and extraterminal (BET) proteins: biological functions, diseases, and targeted therapy. *Signal Transduct Target Ther*. 2023;8(1):420.
31. Jakobsen ST, Jensen RAM, Madsen MS, Ravnsborg T, Vaagenso CS, Siersbaek MS, Einarsson H, Andersson R, Jensen ON, Siersbaek R. MYC activity at enhancers drives prognostic transcriptional programs through an epigenetic switch. *Nat Genet*. 2024;56(4):663–674.

32. Mayer IA, Abramson VG, Lehmann BD, Pietenpol JA. New strategies for triple-negative breast cancer–deciphering the heterogeneity. *Clin Cancer Res*. 2014;20(4):782–790.
33. Li K, Li J, Li Z, Men L, Zuo H, Gong X. Cisplatin-based combination therapies: Their efficacy with a focus on ginsenosides co-administration. *Pharmacol Res*. 2024;203:107175.
34. Gupta S, Nair N, Hawaldar RW, Joshi S, Gulia S, Shet T, Sarin R, Parmar V, Desai S, Ghosh J, et al. Addition of Carboplatin to Sequential Taxane-Anthracycline Neoadjuvant Chemotherapy in Triple-Negative Breast Cancer: A Phase III Randomized Controlled Trial. *J Clin Oncol*. 2026;44(1):9–19.
35. Zhang J, Lin Y, Sun XJ, Wang BY, Wang ZH, Luo JF, Wang LP, Zhang S, Cao J, Tao ZH, et al. Biomarker assessment of the CBCSG006 trial: a randomized phase III trial of cisplatin plus gemcitabine compared with paclitaxel plus gemcitabine as first-line therapy for patients with metastatic triple-negative breast cancer. *Ann Oncol*. 2018;29(8):1741–1747.
36. Borck PC, Guo LW, Plutzky J. BET Epigenetic Reader Proteins in Cardiovascular Transcriptional Programs. *Circ Res*. 2020;126(9):1190–1208.
37. Anichini A, Molla A, Nicolini G, Perotti VE, Sgambelluri F, Covre A, Fazio C, Lofiego MF, Di Giacomo AM, Coral S, et al. Landscape of immune-related signatures induced by targeting of different epigenetic regulators in melanoma: implications for immunotherapy. *J Exp Clin Cancer Res*. 2022;41(1):325.
38. Choo J, Sargsyan A, Khachatryan V, Lonardi S, Pietrantonio F, Sundar R, Klempner S, Janjigian Y. Advances in the management of metastatic gastric cancer: current strategies and emerging therapeutics. *Nat Rev Clin Oncol*. 2026;23(6):441–458.
39. Petitprez F, Levy S, Sun CM, Meylan M, Linhard C, Becht E, Elarouci N, Tavel D, Roumenina LT, Ayadi M, et al. The murine Microenvironment Cell Population counter method to estimate abundance of tissue-infiltrating immune and stromal cell populations in murine samples using gene expression. *Genome Med*. 2020;12(1):86.
40. Chen Y, Qin H, Li N, Wei Y, Lin Y, Deng R, Ding H, Lv Y, Ma T, Li R, et al. Neoadjuvant chemotherapy by liposomal doxorubicin boosts immune protection of tumor membrane antigens-based nanovaccine. *Cell Rep Med*. 2025;6(1):101877.
41. Subramanian A, Tamayo P, Mootha VK, Mukherjee S, Ebert BL, Gillette MA, Paulovich A, Pomeroy SL, Golub TR, Lander ES, et al. Gene set enrichment analysis: a knowledge-based approach for interpreting genome-wide expression profiles. *Proc Natl Acad Sci U S A*. 2005;102(43):15545–15550.
42. Hegde S, Giotti B, Soong BY, Halasz L, Le Berichel J, Schaefer MM, Kloeckner B, Mattiuz R, Park MD, Magen A, et al. Myeloid progenitor dysregulation fuels immunosuppressive macrophages in tumours. *Nature*. 2025;646(8087):1214–1222.
43. Tran MA, Cho BA, Izadmehr S, Yoo SK, Youssef D, Anker JF, Farkas AM, Figueiredo I, Lee K, Ananthanarayanan A, et al. A Tumor-Promoting Inflammatory SPP1 + Macrophage-IL6-CRP Axis Drives Immune Dysfunction in Bladder Cancer. *Cancer Discov*. 2026;16(6):1126–1151.
44. van Elsas MJ, Middelburg J, Labrie C, Roelands J, Schaap G, Sluijter M, Tonea R, Ovcinnikovs V, Lloyd K, Schuurman J, et al. Immunotherapy-activated T cells recruit and skew late-stage activated

M1-like macrophages that are critical for therapeutic efficacy. *Cancer Cell*. 2024;42(6):1032–1050 e1010.

45. Chen S, Saeed A, Liu Q, Jiang Q, Xu H, Xiao GG, Rao L, Duo Y. Macrophages in immunoregulation and therapeutics. *Signal Transduct Target Ther*. 2023;8(1):207.
46. Mehrotra P, Ravichandran KS. Drugging the efferocytosis process: concepts and opportunities. *Nat Rev Drug Discov*. 2022;21(8):601–620.
47. Kong Q, Xia S, Pan X, Ye K, Li Z, Li H, Tang X, Sahni N, Yi SS, Liu X, et al. Alternative splicing of GSDMB modulates killer lymphocyte-triggered pyroptosis. *Sci Immunol*. 2023;8(82):eadg3196.
48. Xia Y, Sun M, Huang H, Jin WL. Drug repurposing for cancer therapy. *Signal Transduct Target Ther*. 2024;9(1):92.

Figures

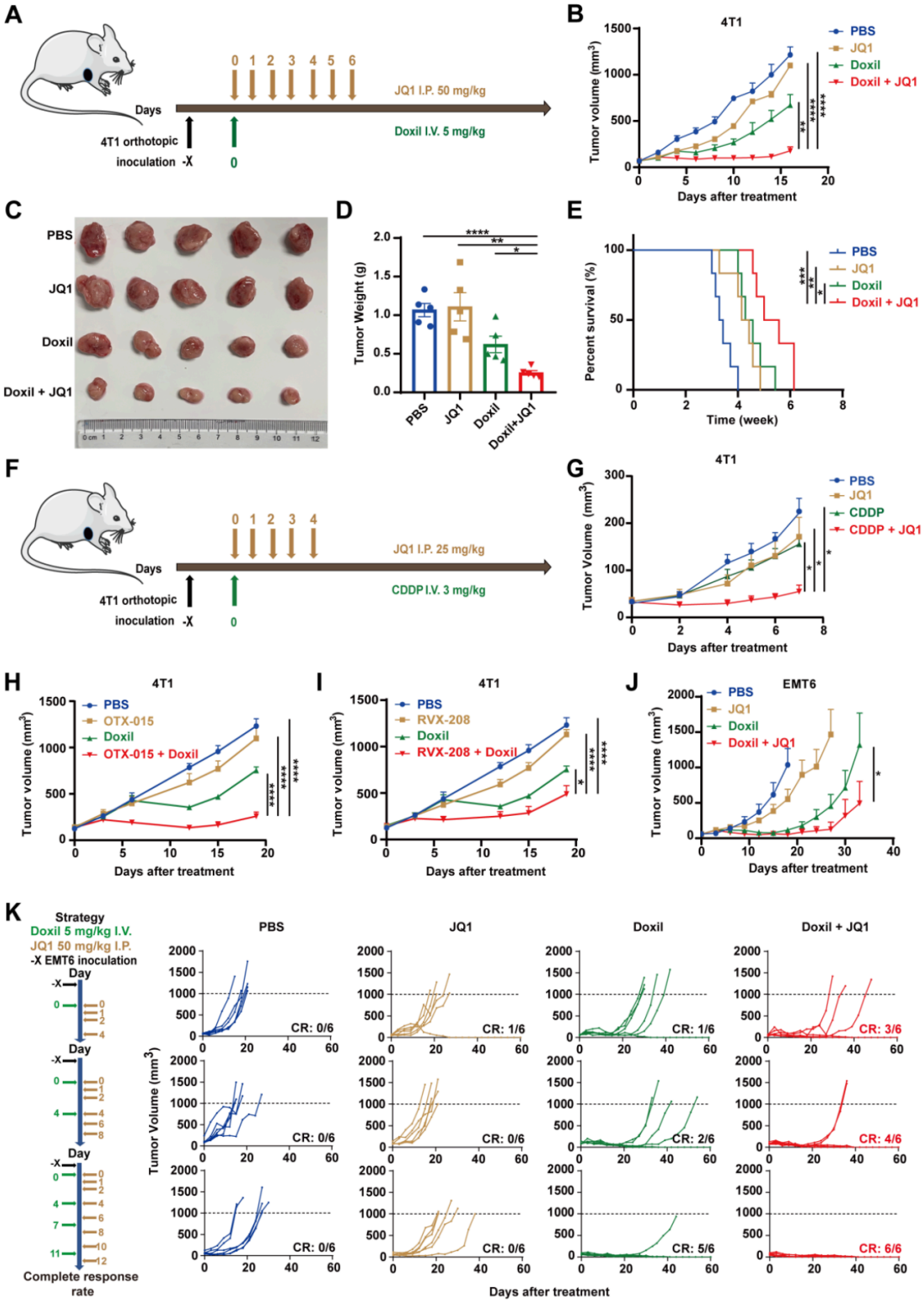


Figure 1

Combination therapy with the chemotherapeutic agent Doxil and BET inhibitors (BETi) significantly suppresses tumor growth. (A) Schematic of the treatment regimen for Doxil combined with JQ1 in the orthotopic 4T1 TNBC mouse model; **(B-E)** Tumor growth (B), the photograph of collected tumors (C), tumor weight (D) (n = 5) and survival curves (n = 6); (E) of 4T1 orthotopic tumor-bearing mice treated with Doxil plus JQ1; **(F)** Schematic of the treatment regimen for CDDP combined with JQ1 in the

orthotopic 4T1 TNBC mouse model; **(G)** Tumor growth of 4T1 orthotopic tumor-bearing mice treated with CDDP plus JQ1 (n = 5); **(H-I)** Tumor growth curves of 4T1 tumor-bearing mice treated with Doxil combined with OTX-015 or RVX-208 (n = 5); **(J)** Tumor growth curves of EMT6 tumor-bearing mice treated with Doxil plus JQ1 (n = 6); **(K)** Tumor growth curves of EMT6 tumor-bearing mice treated with different Doxil-JQ1 combination regimens (n = 6), CR: Complete Response.The data are presented as the mean ± SEM, ns: not statistically significant; * *P* <0.05; ** *P* <0.01; *** *P*<0.001; **** *P* <0.0001.

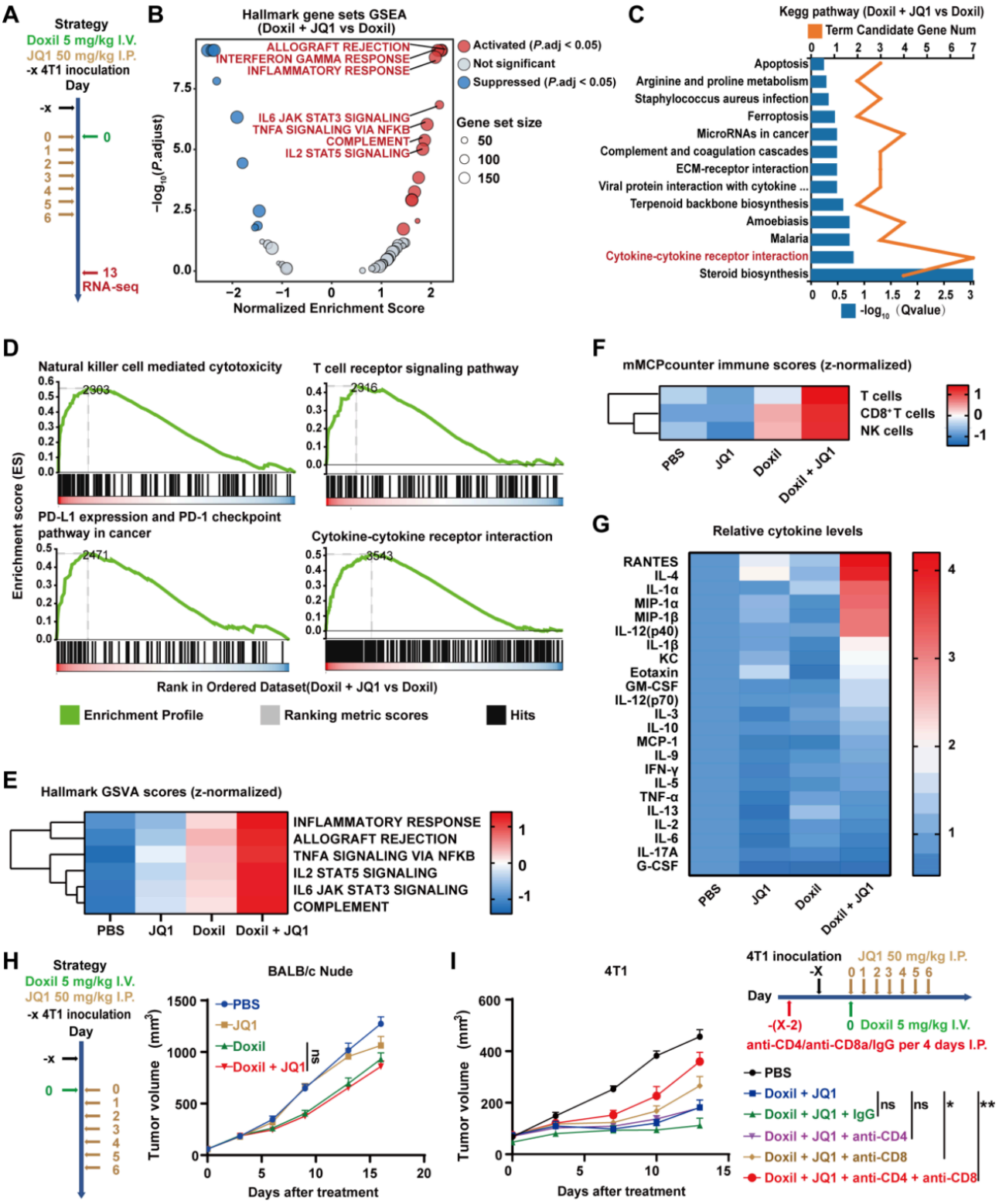


Figure 2

The combination of Doxil and JQ1 enhances intratumoral immune signaling, promotes cytokine secretion, and potentiates antitumor immune responses. (A) Schematic diagram of sampling time point for RNA-seq analysis; **(B)** Bubble plot of GSEA enrichment analysis (Hallmark gene sets) showing immune-related pathways were significantly enriched in the Doxil plus JQ1 group versus Doxil alone; **(C)**KEGG pathway analysis identified significantly enriched differentially expressed genes (DEGs) in tumor tissues of 4T1 tumor-bearing mice treated with Doxil plus JQ1 compared with Doxil group; **(D)** GSEA plot showing KEGG pathway enrichment analysis of tumors from 4T1 tumor-bearing mice treated with Doxil plus JQ1 compared with the Doxil group; **(E)** GSVA was performed to calculate enrichment scores of Hallmark gene sets, and pathway enrichment was compared among PBS, JQ1, Doxil, and Doxil plus JQ1 groups (n = 3); **(F)**Z-normalized immune cell infiltration scores were quantified using mMCPcounter, and the abundance of T cells, CD8+ T cells, and NK cells was compared among the PBS, JQ1, Doxil, and Doxil plus JQ1 treatment groups (n = 3); **(G)**Cytokine array analysis quantified cytokine levels in tumor treated with PBS, JQ1, Doxil and Doxil plus JQ1 (n = 3); **(H)** Tumor growth curves of 4T1 tumor-bearing nude mice after different treatment (n = 5); **(I)** Tumor growth curves of 4T1 tumor following antibody-mediated depletion of CD4/CD8+ T cells and subsequent treatment with Doxil plus JQ1 (n = 6). The data are presented as the mean ± SEM, ns: not statistically significant; * P <0.05; ** P <0.01; *** P<0.001; **** P <0.0001.

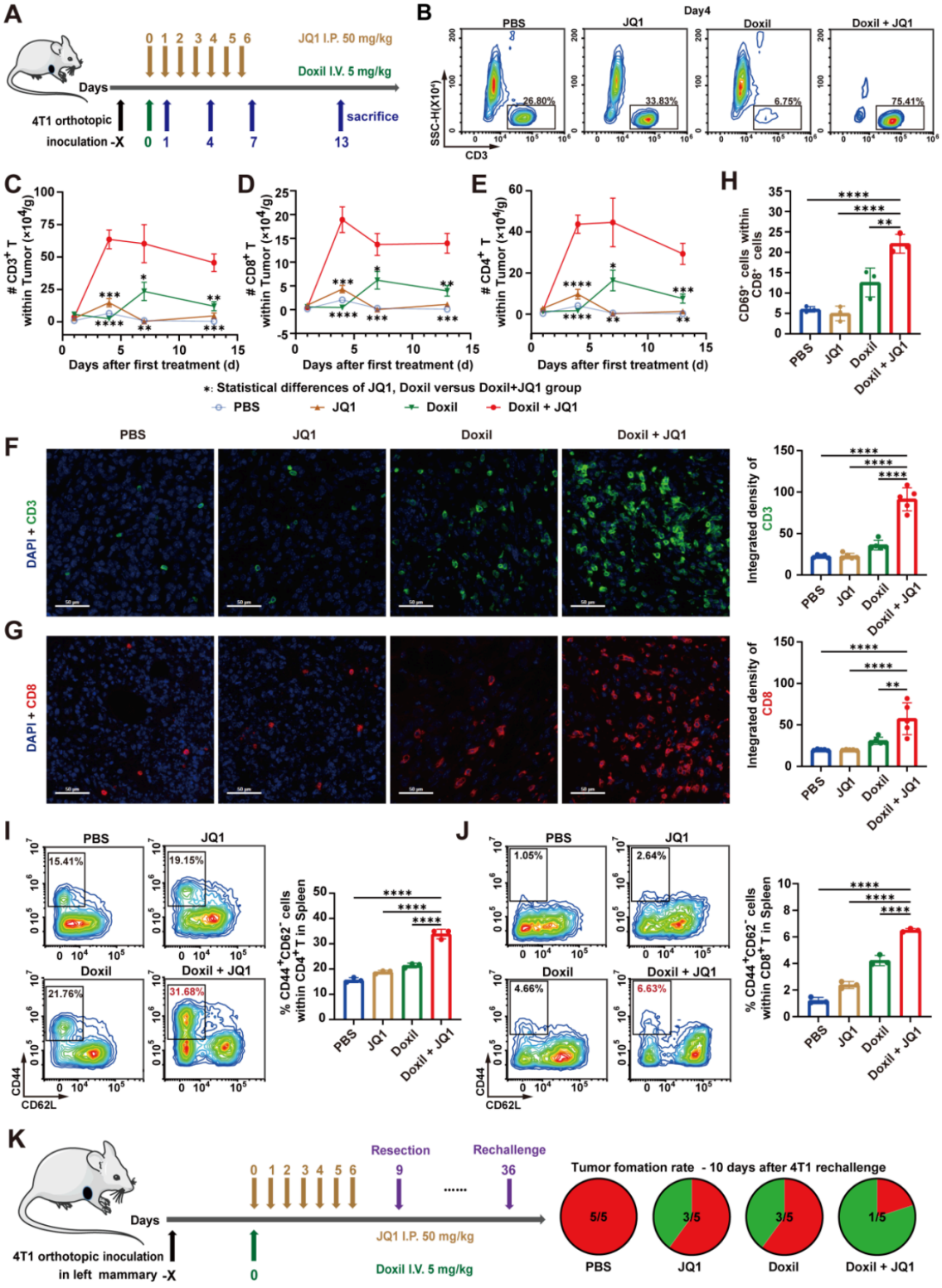


Figure 3

The combination of Doxil with JQ1 enhances T cell infiltration, functional activity, and induces antitumor immune memory in TNBC. (A) Schematic diagram of the Doxil+JQ1 combination therapy regimen and the time points for tumor sample collection in the orthotopic 4T1 TNBC mouse model; **(B-C)** Flow cytometry analysis of the temporal dynamic changes in $CD3^+$ T cell numbers in tumor tissues (C) and the gating plot of $CD3^+$ T cells on day 4 (B); **(D-E)** Flow cytometry analysis of the temporal dynamic

changes in $CD8^+$ T cells (D) and $CD4^+$ T cells (E) numbers; **(F-G)** Immunofluorescence images and quantitative statistical results showed the infiltration of $CD3^+$ T cells and $CD8^+$ T cells in tumor tissue on day 13 after treatment (scale bar = 50 μm); **(H)** Flow cytometry detection of the expression level of CD69 of $CD8^+$ T cells on day 13 post-treatment (n = 5); **(I-J)** Flow cytometry analysis of the numbers of $CD4^+$ effector memory T cells ($CD44^+$ $CD62L^-$) (I) and $CD8^+$ effector memory T cells ($CD44^+$ $CD62L^-$) (J) in the spleen on day 13 post-treatment; **(K)** Schematic diagram of the immune memory challenge experiment design and the tumor formation rate of 4T1 tumor-bearing mice in different treatment groups after rechallenge (n = 5). Data are presented as mean ± standard deviation; ns: not statistically significant; * $P < 0.05$; ** $P < 0.01$; *** $P < 0.001$; **** $P < 0.0001$.

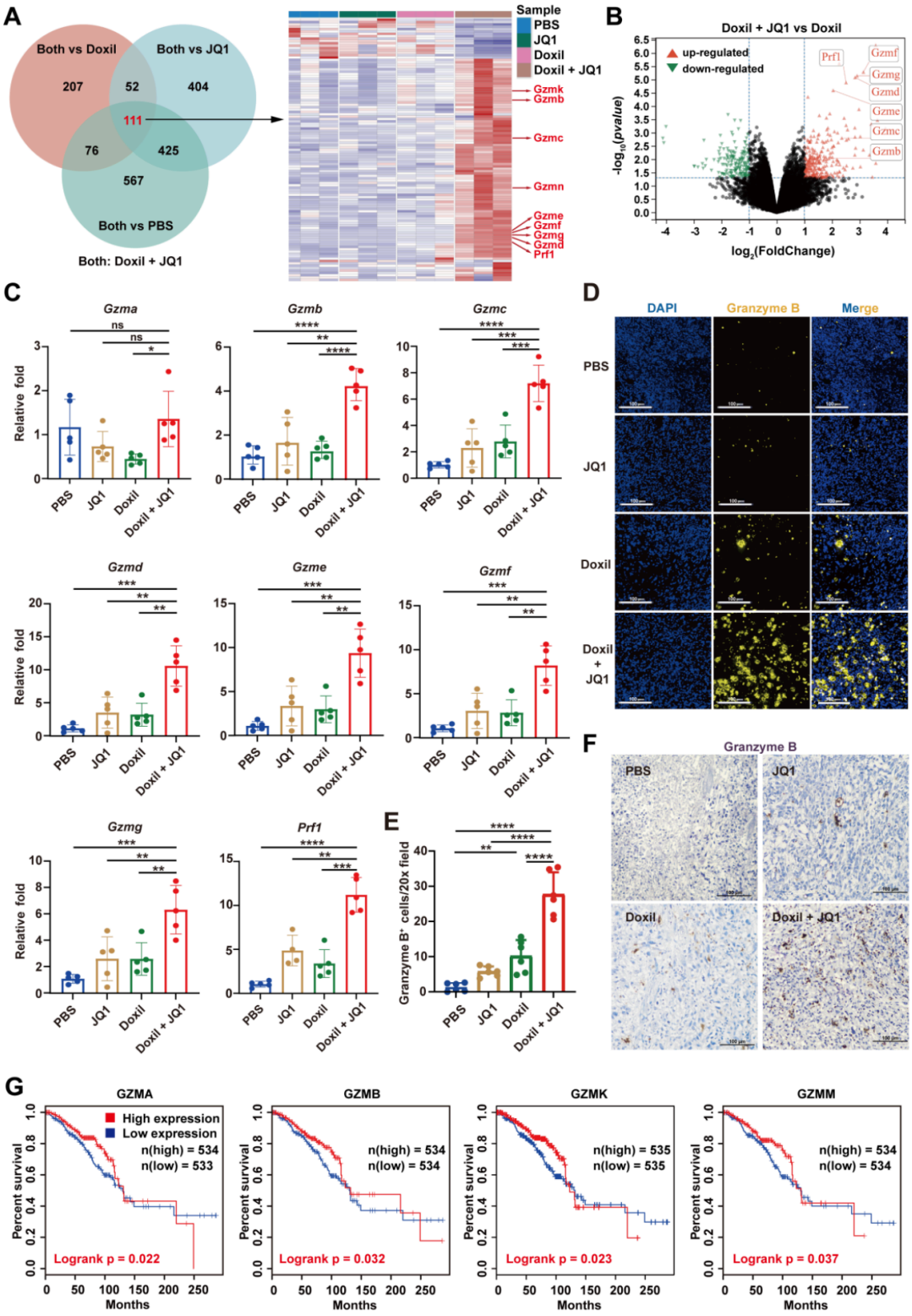


Figure 4

The combination of Doxil and JQ1 enhances the transcription, expression, and secretion of granzyme family genes. (A-B) Differentially expressed genes in tumor tissues of 4T1 tumor-bearing mice on day 13, identified by RNA sequencing (n = 3); **(C)** qRT-PCR analysis of the expression of granzyme family-related genes in tumor tissues on day 9 (n = 5); **(D)**Immunofluorescence assay for the expression level of Granzyme B in tumor tissue samples; **(E-F)** Immunohistochemical staining results (E) and statistical

analysis (F) of Granzyme B (n = 5); scale bar = 100 μm; **(G)** Correlation between the expression of granzyme family genes and the prognosis of TNBC patients in TCGA database. Data are presented as mean ± standard deviation; ns: not statistically significant; * $P < 0.05$; ** $P < 0.01$; *** $P < 0.001$; **** $P < 0.0001$.

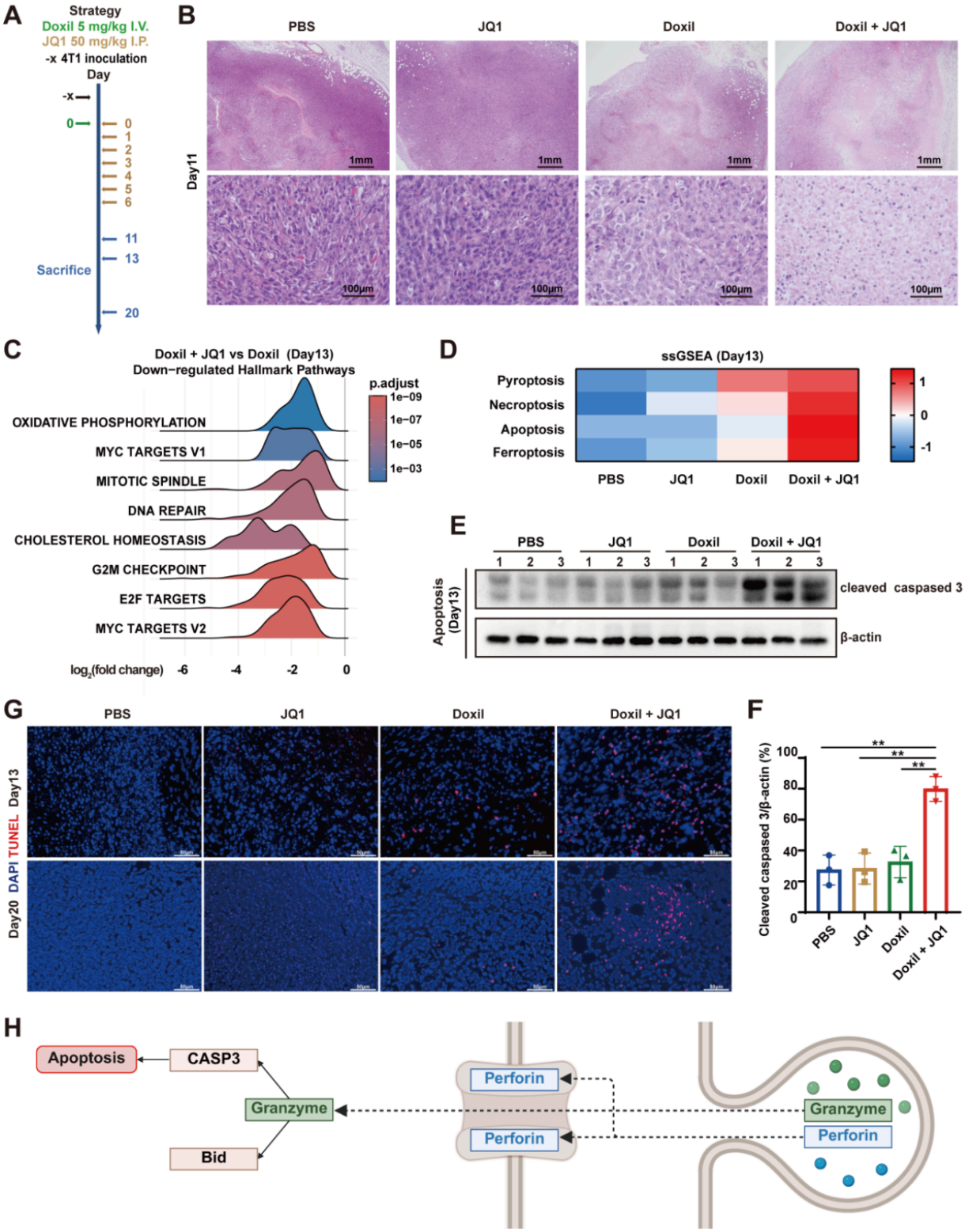


Figure 5

Doxil combined with JQ1 enhances intratumoral apoptosis. (A) Schematic diagram of the Doxil+JQ1 combination therapy and the time points for tumor sample collection to verify tumor cell death; **(B)** H&E staining to observe the pathological changes of tumor tissues on day 11; **(C)** Ridge plot showing all downregulated signaling pathways in GSEA of Hallmark gene sets in the Doxil+JQ1 group compared with the Doxil monotherapy group (n = 3);**(D)** ssGSEA results on day 13 showing the enrichment levels of cell death-related pathways (n = 3); **(E-F)** Western blot analysis of the expression level of cleaved caspase 3 in tumor tissues on day 13 (n = 3); **(G)**TUNEL staining to assess apoptosis in tumor tissues on days 13 and 20, scale bars = 50 μm. **(H)** Schematic representation of the Granzyme and apoptosis-related pathways from the KEGG database. Data are presented as mean ± standard deviation; ns: not statistically significant;

Supplementary Files

This is a list of supplementary files associated with this preprint. Click to download.

- SUPPLEMENTARYMATERIALSCommunicationsMedicine.docx
- FullunedítedblotforFigure5.pdf